Society For Biomaterials

Biomimetic sponges for regeneration of skeletal muscle following trauma

Gabriel J. Haas,[1†] Andrew J. Dunn,[1†] Madison Marcinczyk,[1] Muhamed Talovic,[1] Mark Schwartz,[1] Robert Scheidt,[1] Anjali D. Patel,[1] Katherine R. Hixon,[1] Hady Elmashhady,[1] Sarah H. McBride-Gagyi,[2] Scott A. Sell,[1] Koyal Garg[1]

[1]Department of Biomedical Engineering, Parks College of Engineering, Aviation, and Technology, Saint Louis University, St. Louis, Missouri, 63103
[2]Department of Orthopedic Surgery, Saint Louis University, St. Louis, Missouri, 63103

Received 18 May 2018; revised 17 August 2018; accepted 21 August 2018
Published online 00 Month 2018 in Wiley Online Library (wileyonlinelibrary.com). DOI: 10.1002/jbm.a.36535

Abstract: Skeletal muscle is inept in regenerating after traumatic injuries due to significant loss of basal lamina and the resident satellite cells. To improve regeneration of skeletal muscle, we have developed biomimetic sponges composed of collagen, gelatin, and laminin (LM)-111 that were crosslinked with 1-ethyl-3-(3-dimethyl aminopropyl) carbodiimide (EDC). Collagen and LM-111 are crucial components of the muscle extracellular matrix and were chosen to impart bioactivity whereas gelatin and EDC were used to provide mechanical strength to the scaffold. Morphological and mechanical evaluation of the sponges showed porous structure, water-retention capacity and a compressive modulus of 590–808 kPa. The biomimetic sponges supported the infiltration and viability of C_2C_{12} myoblasts over 5 days of culture. The myoblasts produced higher levels of myokines such as VEGF, IL-6, and IGF-1 and showed higher expression of myogenic markers such as MyoD and myogenin on the biomimetic sponges. Biomimetic sponges implanted in a mouse model of volumetric muscle loss (VML) supported satellite, endothelial, and inflammatory cell infiltration but resulted in limited myofiber regeneration at 2 weeks post-injury. © 2018 Wiley Periodicals, Inc. J Biomed Mater Res Part A: 00A: 000–000, 2018.

Key Words: volumetric muscle loss, extracellular matrix, myogenesis

How to cite this article: Haas GJ, Dunn AJ, Marcinczyk M, Talovic M, Schwartz M, Scheidt R, Patel AD, Hixon KR, Elmashhady H, McBride-Gagyi SH, Sell SA, Garg K. 2018. Biomimetic sponges for regeneration of skeletal muscle following trauma. J Biomed Mater Res Part A. 2018:9999:1–12.

INTRODUCTION

Musculoskeletal injuries are among the most common and frequently disabling injuries sustained by athletes and soldiers.[1] Muscle trauma accounts for 50%–70% of total military injuries and complications involving muscle result in approximately 80% of delayed amputations.[2–4] In a recent article, Corona et al. concluded that muscle trauma involving volumetric muscle loss (VML) contributes to >90% of muscle conditions that result in long-term disability in patients who have been medically retired because of injury.[5] Muscle damage or impaired muscle function is often a secondary complication associated with a broad range of injuries commonly sustained in military conflicts including peripheral nerve injury,[6] tenotomy,[7] ischemia–reperfusion injury,[8] and open fractures.[9] Currently, there are no approved regenerative therapies for the treatment of muscle tissue following VML, presenting a significant opportunity to produce tissue engineered scaffolds for muscle tissue regeneration.

A tissue-engineered scaffold for repair of traumatic muscle injuries should possess adequate mechanical strength and elasticity and should be capable of supporting myoblast proliferation and differentiation. Collagen is a key component of the muscle extracellular matrix (ECM) and has been widely used in the form of gels,[10] electrospun scaffolds,[11] and sponges[12] for skeletal muscle tissue engineering applications. While collagen is highly abundant in almost all tissues, it is a challenging material for scaffold fabrication due to its high hydrophilicity and degradation rate.[13] Laminin (LM) is a heterotrimeric structural protein in the ECM of skeletal muscle fibers that provides an essential scaffold for tissue development, maintenance, and function. Satellite cells are muscle resident stem cells that are mitotically quiescent under normal physiological conditions and reside between the basal lamina and the sarcolemma of the muscle fibers.[14] Satellite cells are highly dependent on the presence of LM in the basal lamina for multiple activities, including proliferation, adhesion, migration, and differentiation within skeletal muscle.[15–18] Stress induced by physical exercise or trauma can trigger satellite cell activation. Following activation, the satellite cells exit their niche to proliferate. They differentiate

†These authors contributed equally to this work.
Correspondence to: Koyal Garg; e-mail: gargk@slu.edu

into myoblasts ($MyoD^+$) that can either fuse with each other to form myotubes ($myogenin^+$, $myosin\ heavy\ chain^+$), or with existing fibers to allow for myofiber repair.[19] The administration of LM-111, an isoform that is present in embryonic tissues but is absent in adult tissues, has demonstrated remarkable regenerative capacity in several models of disease[20–22] and injury,[23–25] primarily by influencing satellite cell activity. However, its efficacy for muscle repair and regeneration has never been evaluated in a VML model.

Gelatin is a denatured form of collagen that retains its biocompatibility and offers a less expensive alternative to collagen.[26] Gelatin sponges have been used in a variety of tissue engineering applications.[26–30] In this study, collagen and LM-111 were chosen to impart bioactivity, and gelatin was used to provide mechanical durability to the biomimetic sponge. To further improve the mechanical properties of the sponges, they were cross-linked using 1-ethyl-3-(3-dimethyl aminopropyl) carbodiimide (EDC). EDC is a non-toxic and biocompatible cross-linking agent that doesn't incorporate into the scaffold but changes into a water-soluble urea derivative that can be easily removed via rinsing.[31,32] The sponges were created by freeze-drying as that is a well-established method for mimicking tissue structural properties.[33] We hypothesized that these biomimetic sponges will serve as ECM analogs at the site of injury and support cellular proliferation, differentiation, and growth factor secretion.[34] The overall goal of this study was to determine the morphological, mechanical, and regenerative properties of these novel biomimetic sponges. The capacity to promote myokine secretion and myogenic protein expression was evaluated by *in vitro* culture with C_2C_{12} myoblasts. Furthermore, the acute *in vivo* myogenic response of the biomimetic sponges was tested in a mouse VML model.

MATERIALS AND METHODS

Fabrication of biomimetic sponges

A 3 wt % porcine skin gelatin (Sigma-Aldrich) solution was prepared in DI water and heated to 60°C. After the gelatin had completely dissolved, the solution was allowed to cool to 50°C. EDC (20 mM) was added to the solution which was vortexed vigorously before being added to square plastic molds (15 × 15 × 5mm, Fisher Scientific). The final concentrations of gelatin, collagen, LM-111 are shown in Table I. Rat tail collagen I (Gibco, 3 mg/mL) solution was added to the molds in gelatin : collagen ratios of 100:0 (pure gelatin), 90:10, and 70:30. LM-111 (Trevigen) was then added to the molds at a final concentration of 50 μg/mL and mixed thoroughly. The molds were placed in a 100% methanol bath, and allowed to gel at 4°C for 30 min, followed by overnight freezing at −8°C. The molds were then moved to a − 80°C freezer for 24 hours. After the molds were removed from the methanol bath, the sponges were frozen for another 24 hours at −80°C. The frozen molds were lyophilized for at least 19 hours. The cross-section of the lyophilized sponges was observed through scanning electron microscopy (SEM). Preliminary studies showed that 60:40, 50:50 gelatin : collagen and pure collagen (100%) sponges did not maintain structural integrity upon hydration and therefore were not included in the study.

TABLE I. Concentration of components used for creating the biomimetic sponges

	Gelatin	Collagen	LM-111	EDC
100%	30 mg/mL	0 mg/mL	50 μg/mL	20 mM
90:10	27 mg/mL	0.3 mg/mL	50 μg/mL	18 mM
70:30	21 mg/mL	0.9 mg/mL	50 μg/mL	14 mM

Water uptake

In order to measure the swelling potential and the mesh-size of the scaffolds, water uptake percentage was calculated by measuring the dry and hydrated weight of each sponge (n = 3) at 5-min time intervals after soaking each sponge in 1 mL of water. The formula used was:

$$\text{Water Uptake Percentage} = \frac{(\text{Hydrated Weight} - \text{Dry Weight})}{\text{Dry Weight}} \text{ x } 100\%$$

μCT analysis

The biomimetic sponges were created in the plastic molds as described above and 6 mm disks were punched using a biopsy punch (n = 3–4). The disks were analyzed using μCT 35 (ScanCo Medical, Wayne, PA) as described previously[35,36] to measure the structural features of the scaffolds under hydrated conditions. The morphological features such as pore-size, heterogeneity, interconnectivity, and void: solid ratio was obtained using the manufacturer installed trabecular morphology analysis. The scaffolds were scanned under the following parameters: X-ray tube potential 45 kVp, X-ray intensity 4 W, isotropic voxel size 7 μm, integration time 600 ms, frame averaging 1, projections 500, and a medium resolution scan. The central area of each scaffold was analyzed using a threshold of 40 per milles (Scanco systems' default unit). A majority of the scaffold was captured for analysis and only a small portion of the outermost layer was excluded. We first analyzed scans from a small subset of each group at a range of thresholds from very low, which would erroneously include void voxels as scaffold, to very high, which would exclude scaffold voxels and count them as space. The selected threshold was determined by graphing the results and looking for an inflection point or min/max within the range across multiple outcomes. This indicates the point at which most of the voxels are correctly assigned. Therefore, voxels above the threshold of 40 per milles were considered scaffold, and those below were considered void space.

Biodegradation of the biomimetic sponges

Dry sponge disks (6 mm) were weighed, immersed in 800 μL of phosphate buffered saline (PBS) in a 24 well plate and maintained in an incubator at 37°C for 1 week. The disks were removed and lyophilized at the end of 1 week to measure the remaining dry weight.[37] The PBS solution was collected for pH analysis.

Mechanical testing

Compression testing was performed using an MTS Criterion Model 42. The sponges were prepared in square plastic molds of dimensions 25 × 20 × 5mm (n = 4) and were first tested while dry, and then tested again after being hydrated in 3 mL of DI water for 5 min. A strain rate of 10 mm/min was used until a strain percentage of 50% was reached. The peak stress, peak load, compressive modulus values were obtained from MTS software (MTS TestSuite: TW Elite) using the stress–strain curve. It should be noted that the sample dimensions do not conform to the ASTM standard and caution must be observed while making direct comparisons to mechanical properties of other scaffolds.

Cell-culture

The sponges were disinfected in 95% ethanol for 5 min, rinsed twice in 1X phosphate buffer solution (PBS) for 5 min each, followed by overnight incubation at 37°C in 5% CO_2 in growth media (DMEM-F12 containing 10% fetal bovine serum (FBS), 10% horse serum (HS), and 1% penicillin–streptomycin). C_2C_{12} myoblasts (ATCC) were seeded on the sponges at a density of 500,000 cells/well in a 12 well plate for 5 days (n = 3–4) in the growth media. The growth media was replaced every alternate day. Cell culture supernatants and cellular protein lysates were collected on day 1 and 5. Supernatants were also collected from myoblasts cultured at the same cell-density on tissue culture plastic (TCP) for comparison. The production of vascular endothelial growth factor (VEGF), interleukin-6 (IL-6), and insulin-like growth factor (IGF)-1 by C_2C_{12} myoblasts was quantified in cell-culture supernatants using ELISA (Peprotech) as per manufacturer's instructions.

Implantation of biomimetic sponges in a VML model

This work was conducted in compliance with the Animal Welfare Act, the implementing Animal Welfare Regulations, and in accordance with the principles of the Guide for the Care and Use of Laboratory Animals. All animal procedures were approved by the Saint Louis University's Institutional Animal Care and Use Committee.

Male C57BL6 mice (5 weeks old) were purchased from Charles Laboratory and housed in a vivarium accredited by the Association for Assessment and Accreditation of Laboratory Animal Care International and provided with food and water *ad libitum.* The animals were weighed prior to surgery and anesthetized using 2.5% isoflurane. The surgical site was aseptically prepared, and sustained release buprenorphine (1 mg/kg) was injected in the nape of the neck prior to the procedure. A lateral incision was made through the skin to reveal the gastrocnemius-soleus (GAS) complex. The skin was separated from the musculature by blunt dissection. A metal plate was inserted underneath the GAS muscle, and a 3-mm punch biopsy was performed to remove approximately ~10% of the muscle mass. The biopsy was removed and weighed for consistency (Table II). A subset of VML injured muscles received a 3-mm disk of the 70:30 biomimetic sponge (n = 6), while others were left untreated (n = 4). Bleeding was controlled with light pressure, and the skin incision was closed with simple interrupted sutures. The animals were allowed to recover for 2 weeks and euthanized via CO_2 asphyxiation. GAS muscles were weighed upon collection and processed for histological and biomolecular analyses.

Western blotting

The protein expression was evaluated in both *in vitro* cell culture samples and the hindlimb muscle samples using western blotting. Protein lysates from myoblasts cultured on both sponges and TCP were collected on days 1 and 5 of cell culture and were quantified for myogenic markers using western blotting as previously described.[38,39] Briefly, acellular and myoblast-seeded sponges were rinsed twice in PBS, and the cellular protein lysates were collected in RIPA buffer with protease inhibitor cocktail (Sigma). GAS muscles were homogenized in the same buffer to collect muscle protein lysates. The protein concentration was determined using the Pierce BCA protein assay kit (Thermo Scientific). Cellular protein lysates (20 μg) and muscle protein lysates (60 μg) were mixed with laemmli buffer, denatured and resolved by SDS-polyacrylamide gel electrophoresis (SDS-PAGE) using 4–20% gels (Bio-rad) and transferred onto nitrocellulose membranes. Equal protein loading was verified by Ponceau S staining. The membranes were probed using anti-desmin (Abcam), anti-MyoD (Thermo Fisher Scientific), anti-myogenin (Millipore), anti-GAPDH (Cell Signaling), anti-α-actinin (Cell Signaling), anti-HSP70 (Cell Signaling), anti-iNOS (Abcam), anti-tranforming growth factor beta 1 receptor (TGF-β1R, Millipore), anti-interleukin 10 (IL-10, Millipore), and appropriate HRP-conjugated secondary antibodies.

Histology

The sponges were removed from cell culture media on day 5 of culture, immersed in optimal cutting temperature (OCT) compound and frozen in liquid nitrogen for cryosectioning. The cross-sections of sponges were stained with hematoxylin and eosin (H&E) and DAPI to assess cellular infiltration in their three-dimensional structure. The $DAPI^+$ nuclei were quantified as the percentage of area fraction in ImageJ from 6–7 nonoverlapping 40× images (Zeiss Axiocam) of the sections, using a thresholding method adopted previously.[39–41]

GAS muscles were weighed upon collection and frozen in 2-methyl butane (Fisher Scientific) that was super-cooled in a liquid nitrogen bath. The muscles were mounted on stubs using OCT and cryosectioned. Cross-sections (n = 3–4) were stained with H&E, anti-Pax7 (Abcam), Collagen I (Abcam),

TABLE II. Morphological characteristics of the VML injured muscles

	Biopsy weight (mg)	Muscle weight (g)	Body weight (g)	MW/BW (mg/g)
No treatment (n = 4)	10.96 ± 2.18	0.1172 ± 0.027	21.45 ± 3.1897	5.40 ± 0.25
Biomimetic sponge (n = 6)	11.66 ± 1.71	0.1225 ± 0.027	21.73 ± 3.3260	5.61 ± 0.26

MF20 (R&D systems), F4/80 (Invitrogen), and CD31 (R&D systems). Appropriate fluorochrome-conjugated secondary antibodies (Invitrogen) were as described previously.[38,39] Images were captured at 10× or 40× magnification using a Zeiss Axiocam microscope. Quantitative analysis was performed in ImageJ as described previously.[39] The quantification of myofibers with centrally located nuclei was done manually in ImageJ by taking non-overlapping images of the entire muscle section (n = 4–6/group). The counts were normalized to the manually measured area of the muscle section. The COL: MHC ratio was determined using ImageJ from 3 nonoverlapping images of the defect region (n = 3–5/group) using a thresholding method described previously.[39]

Statistical analysis

All data is presented as means ± SEM. Data were analyzed and graphed using GraphPad Prism 6 for windows. A one-way or two-way ANOVA was performed on most data to determine whether a significant interaction or main effect existed between factors for each dependent variable under consideration. When appropriate, a least significant difference (LSD) post hoc comparison was performed to identify the source of significance with $p \leq 0.05$. The *in vivo* data was analyzed using an unpaired student t test.

RESULTS

Morphological characterization of the biomimetic sponges

The SEM micrographs of the cross-sections of the biomimetic sponges at 500 × and 1500 × magnifications are shown in Figure 1(A). The addition of collagen appeared to increase the overall porous structure and void space in the sponges. The water uptake capacity was 766% for pure gelatin, 1037% for 90:10 and 1216% for 70:30 sponges [Fig. 1(B)]. The water uptake percentage of the 70:30 biomimetic sponges was significantly different from the 100% pure gelatin sponges between 15–30 min (ANOVA; interaction p = 0.9985, group p = <0.0001, time p = <0.0001). The weight of the sponges decreased over the 1-week period in the incubator but about ~66–77% of their original weight was retained and they appeared structurally intact [Fig. 1(C)]. The pH changed during this time from 7.3 to 6.8 in all cases. This drop in pH could be attributed to the degradation products or the dissolution of CO_2 in PBS.[37]

To further illustrate the pore-size of the morphological properties of the biomimetic sponges, we performed a quantitative analysis of the scaffolds using μCT. The 3D reconstruction of the sponges scanned using μCT is shown in Figure 2(A). The average pore-diameter of the sponges ranged between 63–84 μm. While the 70:30 sponges had the smallest pore-diameter, they showed the highest interconnectivity between pores [Fig. 2(C)]. The void : solid ratio was determined to be ~0.93, suggesting that about 7% of the total space in the sponges is the actual scaffold [Fig. 2 (D)]. The pore-heterogeneity was highest on the 90:10 sponges, suggesting a wide range of pore-sizes [Fig. 2(E)]. The 70:30 sponges showed the highest water uptake capacity [Fig. 1(B)], which could be attributed to a highly interconnected network of pores in the 70:30 sponge as shown by the μCT analysis.

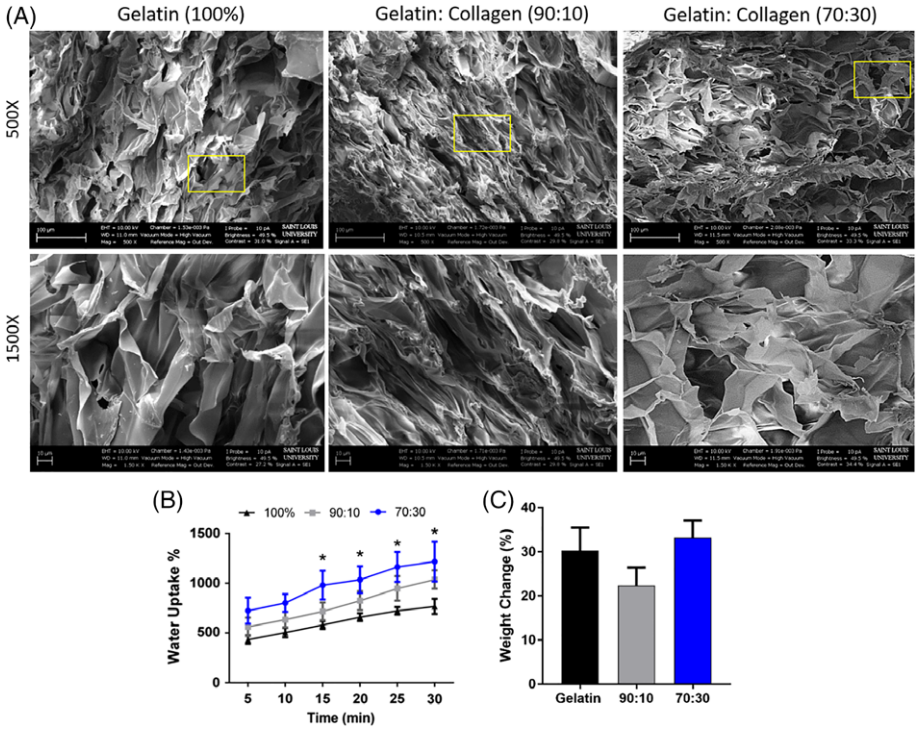

FIGURE 1. (A) Cross-sections of the sponges imaged by scanning electron microscopy are shown at 500× and 1500×. The square boxes approximate the magnified area. (B) The water uptake capacity of the sponges, and (C) the percentage of weight lost over a week at 37°C.

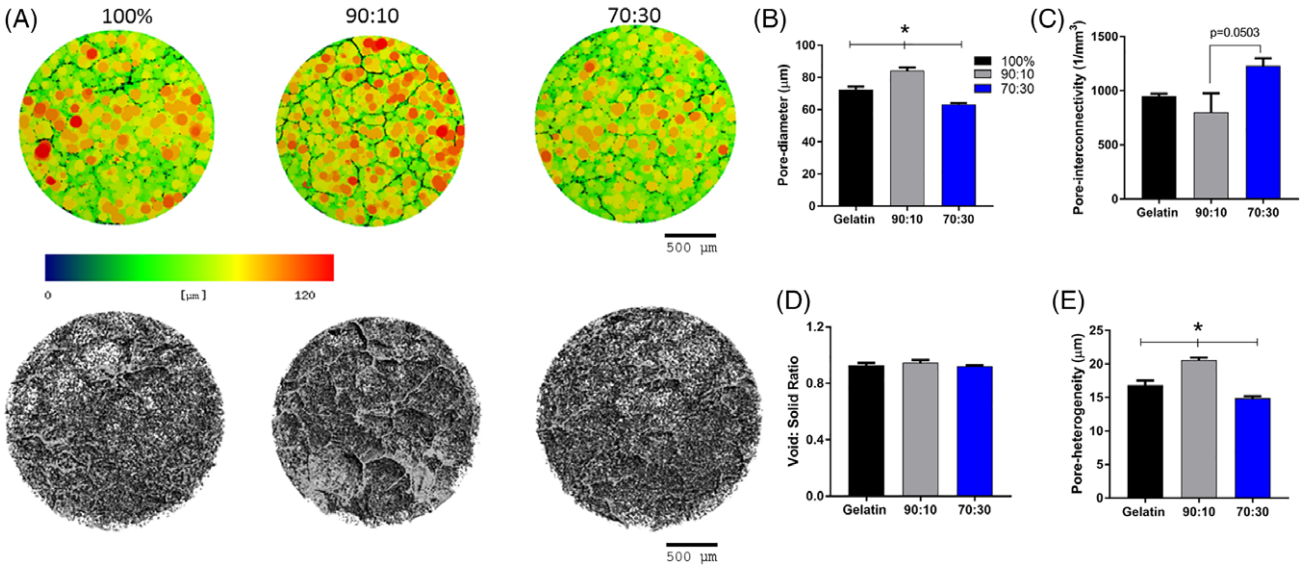

FIGURE 2. (A) 3D reconstructed cross-section of the biomimetic sponges that were analyzed using μCT. The color bar denotes the size of the pores. A blue/green voxel is within a "small" pore, and an orange/red voxel is contained within a "large" pore. For this figure blue is 0 μm and red is 120 μm. Quantitative measurements of the scaffold's morphological features such as (B) pore-diameter, (C) pore-interconnectivity, (D) void: solid ratio, and (E) pore-heterogeneity, are presented. The average pore size ranged from ~60–80 μm which would be represented by green/yellow colors in the color bar.

Mechanical properties of the biomimetic sponges

The results of the compression testing are shown in Figure 3(A–C). Making a direct comparison to mechanical properties of other scaffolds[37] is difficult as the sample dimensions and testing parameters would greatly affect the final values.[26] The peak load of the gelatin sponges was determined to be 60 N and the compressive modulus of the pure gelatin sponge was determined to be 808 kPa. Incorporation of 30% collagen in the biomimetic sponges significantly lowered the compressive modulus compared to the gelatin control sponge, suggesting increased compliance. Overall, the hydrated sponges showed a significant decrease in the peak stress (ANOVA; interaction p = 0.1170, group p = 0.1013, hydration p = <0.0001), peak load (ANOVA; interaction p = 0.1236, group p = 0.1120, hydration p = <0.0001), and compressive modulus (ANOVA; interaction p = 0.0251, group p = 0.0253, hydration p = <0.0001) for all groups. The hydrated values were closer to Young's modulus of the native skeletal muscle reported in previous studies (~10 kPa).[42,43]

Cellular growth and infiltration into the biomimetic sponges

The cryosections of the C_2C_{12} myoblast-seeded biomimetic sponges were obtained on day 5. The sections stained with DAPI and H&E are shown in Figure 4(A). The density of cellular nuclei appeared to increase with increasing percentage of collagen in the sponges. The 70:30 sponges showed the highest infiltration of myoblasts into their 3D structure and presented a significantly greater $DAPI^+$ nuclei content per area than the pure gelatin and the 90:10 sponges. The H&E images show the location of cellular nuclei with respect to the scaffold. The C_2C_{12} myoblasts can be seen lining the pores of the sponges, as indicated by the black arrows. Similar to the DAPI stained images, the cellular quantity and overall infiltration increased with increasing concentrations of collagen.

Myogenic protein expression on the biomimetic sponges

The expression of myogenic proteins in C_2C_{12} myoblasts cultured on the sponges as well as TCP is presented in Figure 5

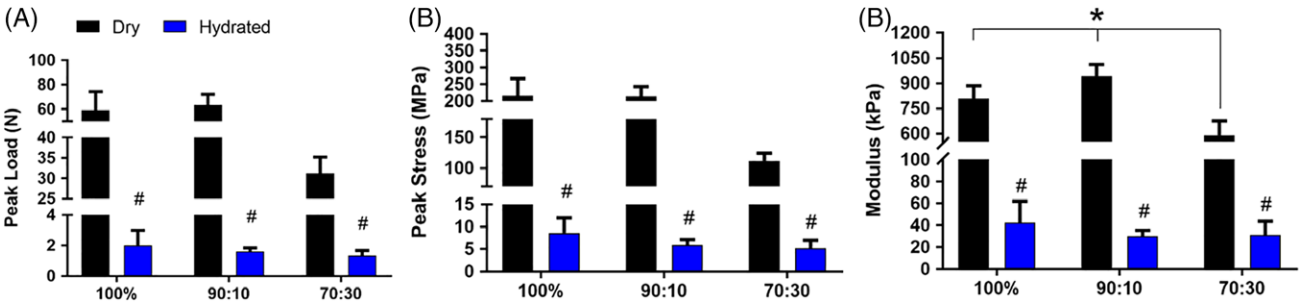

FIGURE 3. Compressive mechanical tests showed reduced (B) peak stress (C) peak load and (D) modulus for the 70:30 biomimetic sponge. Hydration resulted in more compliant scaffolds and statistically different mechanical properties. "*" indicates statistical difference (p < 0.05) among dry biomimetic sponges and "#" indicates statistical difference between dry and hydrated biomimetic sponges.

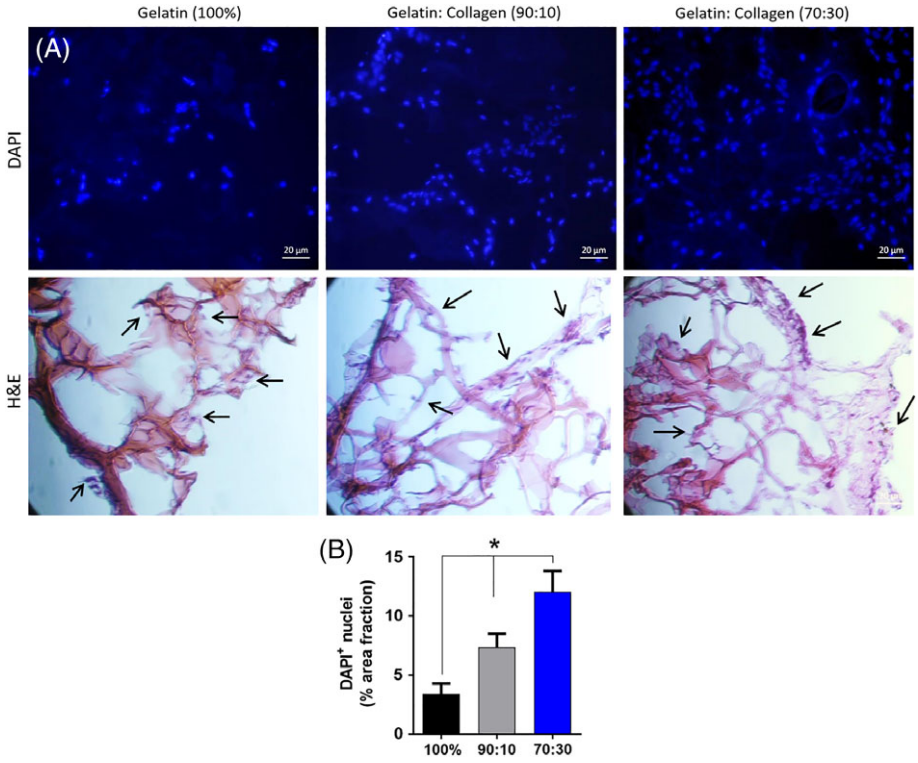

FIGURE 4. (A) Cryo-sections of the sponges were stained with DAPI (top panel) and H&E (bottom panel). (B) The area fraction of DAPI$^+$ nuclei was significantly higher in the 70:30 biomimetic sponges compared to the 100% gelatin and the 90:10 sponges. The black arrows point toward nuclei in the H&E images.

(A). The expression of MyoD trended higher on the 90:10 and 70:30 sponges compared to pure gelatin sponge on day 1. On day 5, MyoD expression significantly increased on the gelatin sponge and TCP compared to day 1 but was not significantly different between the sponges (ANOVA; interaction p = 0.0669, group p = 0.2409, time p = <0.0001). The expression of myogenin showed a linear increase with increasing collagen concentration in the sponges and was significantly higher in the 90:10 and 70:30 sponges compared to 100% gelatin on day 1 (ANOVA; interaction p = 0.0050, group p = <0.0001, time p = <0.0001). The expression of myogenin was not detected on day 1 and was significantly lower on TCP compared to the sponges on day 5. However, a significant increase in myogenin expression was observed on the pure gelatin sponge on day 5 compared to day 1. The expression of α-actinin [Fig. 5(D)] was significantly higher on the TCP compared to the sponges on day 1. The expression of α-actinin was also significantly higher on the 90:10 biomimetic sponge compared to pure gelatin sponge on day 1 but no significant differences were observed on day 5 between the groups (ANOVA; interaction p = 0.0010, group p = 0.0047, time p = 0.0631). No bands were detected in protein lysates collected from acellular sponges.

Secretion of myokines on biomimetic sponges

The ELISA results for VEGF, IL-6, and IGF-1 in cell-culture supernatants are shown in Figure 6. The levels of VEGF and IL-6 released by C_2C_{12} myoblasts increased linearly with increasing percentage of collagen in the biomimetic sponges. The myoblasts cultured on the 70:30 sponges produced the highest quantity of VEGF (ANOVA; interaction p = 0.7000, group p = 0.0003, time p = 0.0002) and IL-6 (ANOVA; interaction p = 0.1502, group p = <0.0001, time p = 0.0687) compared to 100% gelatin sponges at both day 1 and 5. No significant differences were observed in the secretion of IGF-1 by myoblasts (ANOVA; interaction p = 0.0818, group p = 0.3832, time p = 0.2817). The amount of released VEGF was significantly increased on the 90:10 and 70:30 sponges at day 5 compared to day 1 but remained constant on the 100% gelatin sponges. The level of IL-6 trended toward a decrease, but that of IGF-1 trended toward an increase on the 100% gelatin sponges on day 5 of culture.

The myogenic response of biomimetic sponges *in vivo*

Based on the results of the *in vitro* studies, the 70:30 biomimetic sponge was selected for implantation in the mouse VML model. Muscle weights were recorded upon collection, and no statistical difference was found at 2 weeks post-injury (Table II). At 2 weeks post-injury, qualitative immunohistological analyses were performed at the site of the defect. Qualitative analysis of the histological images suggested that the influx of inflammatory cells (F4/80$^+$), endothelial cells (CD31$^+$), and satellite cells (Pax7$^+$) was higher in the biomimetic sponge treated group [Fig. 7(B,D)]. Unlike the untreated VML injured muscles, several small diameter myosin$^+$ myofibers were observed in the biomimetic sponge treated defect site, in close proximity to the remaining muscle mass. The deposition of connective tissue (collagen$^+$ and

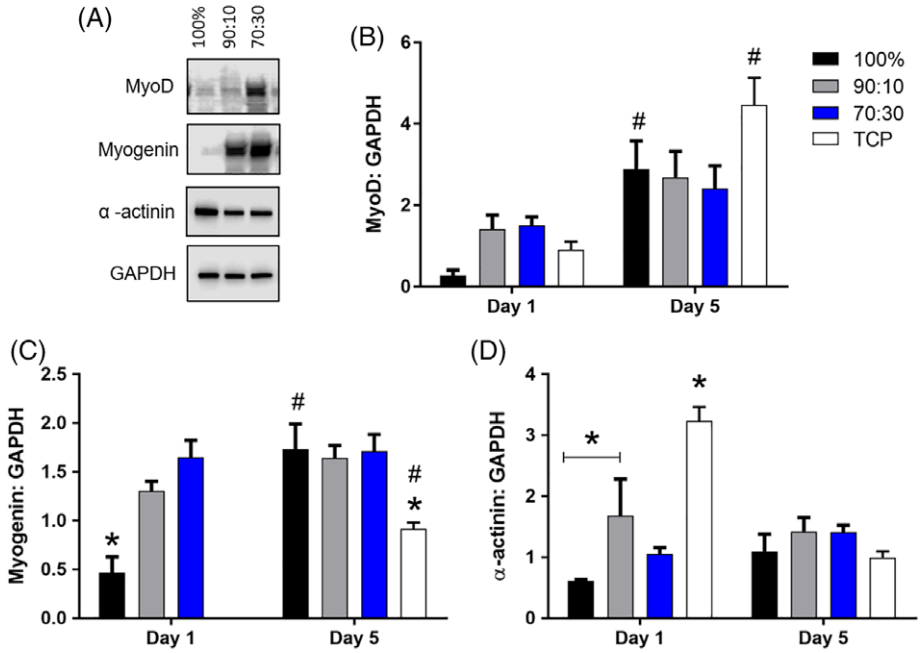

FIGURE 5. (A) Myogenic protein expression was determined by western blotting. The quantification of (B) MyoD, (C) myogenin and (D) alpha-actinin with respect to GAPDH are shown for days 1 and 5. "*" indicates statistical difference ($p < 0.05$) from all other groups at a particular time-point and "#" indicates statistical difference between days 1–5 for a particular group.

laminin^{+}) was similar in both groups. No significant differences were noted [$p = 0.2375$, Fig. 7(E)] in the number of myofibers with a centrally located nuclei between the VML injured and the biomimetic sponge treated muscles. Quantitative analysis of collagen : myosin ratio trended higher on the biomimetic sponge treated VML muscles, but no statistical difference was noted [$p = 0.3118$, Fig. 7(F)].

Skeletal muscle protein lysates from VML injured and biomimetic sponge treated muscles were probed for the following myogenic proteins: MyoD, desmin, myogenin, and α-actinin [Fig. 8(A–D)]. The biomimetic sponge treated muscles showed significantly higher expression of MyoD and desmin compared to untreated muscles. The expression of myogenin trended higher on the biomimetic sponges

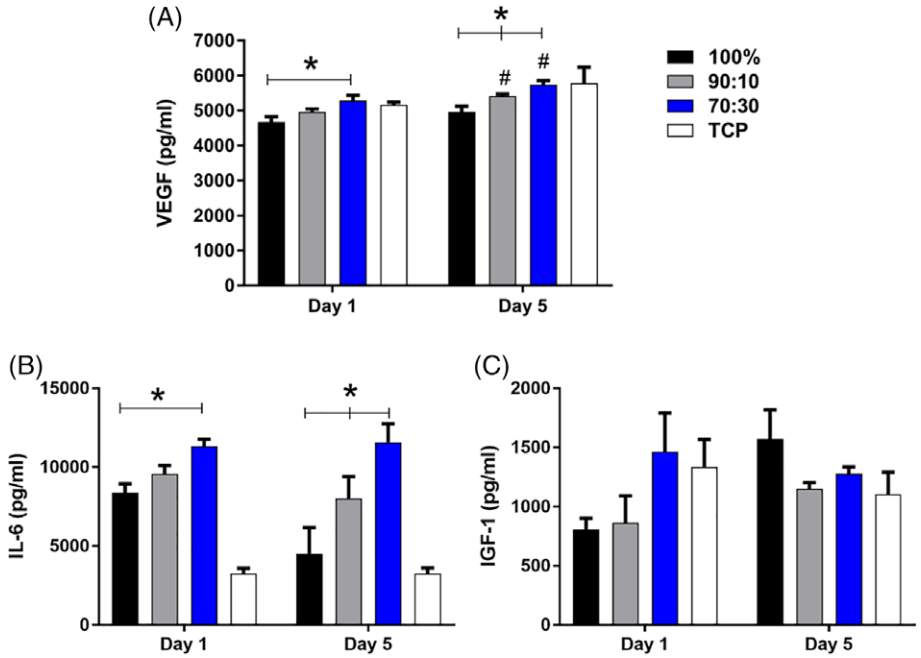

FIGURE 6. Quantification of (A) VEGF, (B) IL-6, and (C) IGF-1 levels produced by myoblasts cultured on the sponges. The 70:30 biomimetic sponges resulted in the highest levels of VEGF and IL-6 production on days 1 and 5. "*" indicates statistical difference ($p < 0.05$) between biomimetic sponges at a particular time-point and "#" indicates statistical difference between days 1–5 for a particular biomimetic sponge.

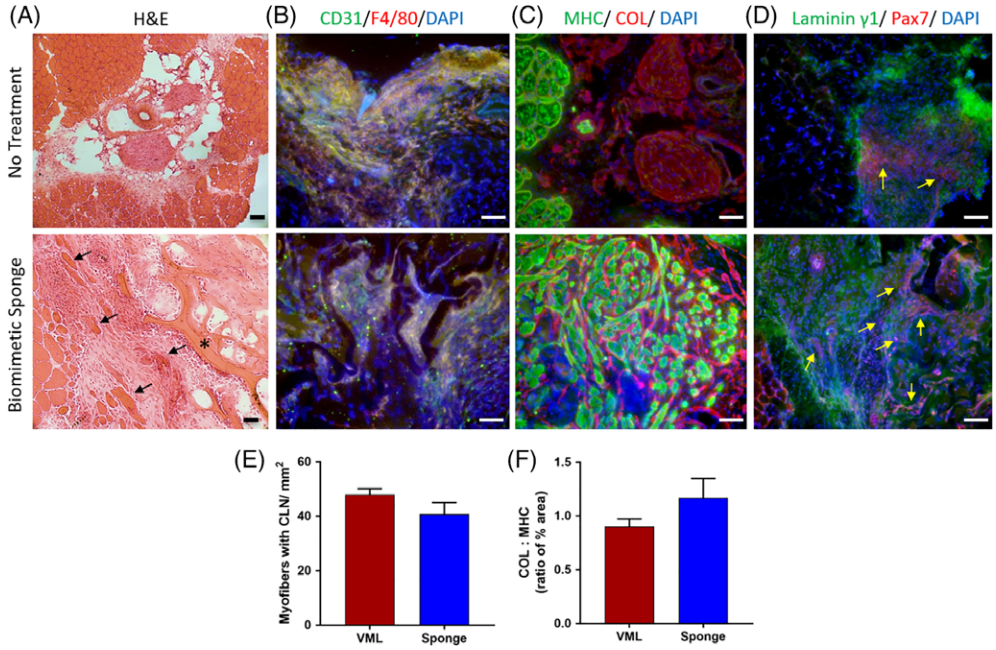

FIGURE 7. The acute response of VML injured muscle to biomimetic sponge implantation. Tissue samples harvested at 2 weeks post-injury were stained for (A) H&E (scale bar =20 μm), black arrows point toward newly regenerated myofibers in the defect region and the asterisks (*) show the biomimetic sponge. (B) F4/80 and CD31 (C) Collagen and Myosin, and (D) Laminin γ1 and Pax7 (scale bar =20 μm), yellow arrows show $Pax7^+$ satellite cells. The histological images were quantified for the (E) total number of myofibers with centrally located nuclei (normalized to the area of the muscle section), and the (F) Collagen : Myosin ratio.

(p = 0.0804) while that of α-actinin was not significantly different between the groups. The expression of heat shock protein (HSP)-70, a protein associated with cellular stress,[44,45] trended lower (p = 0.0820) on the biomimetic sponge treated VML injured muscles [Fig. 8(E)]. Inducible nitric oxide synthase (iNOS) is an enzyme that is primarily expressed on pro-inflammatory macrophages in injured skeletal muscle. The protein expression of iNOS trended higher on the biomimetic sponge treated VML injured muscles [Fig. 8(F)] suggesting heightened inflammation-dependent muscle healing.[46] The expression of arginase, an enzyme associated with anti-inflammatory macrophages was not detected in either VML injured or sponge treated muscles (data not shown). The expression of transforming growth factor beta 1 receptor (TGF-β1R) was similar between both sponge-treated and untreated VML injured muscles [Fig. 8(E)].

DISCUSSION

A clinically approved therapy for repair and regeneration of large muscle defects currently does not exist. Many of the tissue-engineered scaffolds are either mechanically unsuitable or fail to enhance tissue-resident stem cell activity.[12,47,48] We are only aware of one other study where LM-111 was delivered to the site of VML injury using hydrogels composed of hyaluronic acid and poly(ethylene glycol).[49] The study reported little to no cellular infiltration into the defect owing to the largely intact and undegraded hydrogels. The absence of cellular infiltration into the hydrogels was ultimately correlated to lack of myofiber regeneration and functional recovery. The biomimetic sponges described in this study offer several significant improvements over the tissue-engineered biomaterials currently being researched. The biomimetic sponges contain a mixture of two highly pro-regenerative proteins: collagen and LM-111, for stimulating cellular activity. The sponges also contain gelatin which provides mechanical stability and durability without compromising its biocompatibility. These sponges can be fabricated in a variety of shapes and sizes and provide an "off-the-shelf" solution to a variety of wounds/tissue defects. The sponges can be easily fabricated in a short-time frame with commonly available lab equipment. Moreover, pro-regenerative growth factors and biomolecules, as well as pharmaceutical drugs, can also be easily incorporated into the sponges for a sustained and controllable release.[50] Preliminary studies showed that pure gelatin gels did not support myoblast adhesion and growth. Therefore, LM-111 was added to the 100% gelatin sponges to support myoblast adhesion and activity.

A pore-size of about 100 μm is recommended to allow for neovascularization and mass transport through a tissue-engineered scaffold. Typically, biomaterials that exhibit a higher swelling ratio have larger pore-sizes.[51] Our data shows that 70:30 biomimetic sponges swelled the most in water [Fig. 1(B)], suggesting a larger mesh-size. In support, a more open, interconnected, and porous structure of the 70:30 sponges was observed with SEM [Fig. 1(A)] and μCT [Fig. 2(C)]. This interconnected 3D network of pro-regenerative proteins in the 70:30 biomimetic sponges also supported greater myoblast infiltration into the scaffolds, as shown in Figure 4. The highly interconnected pore network

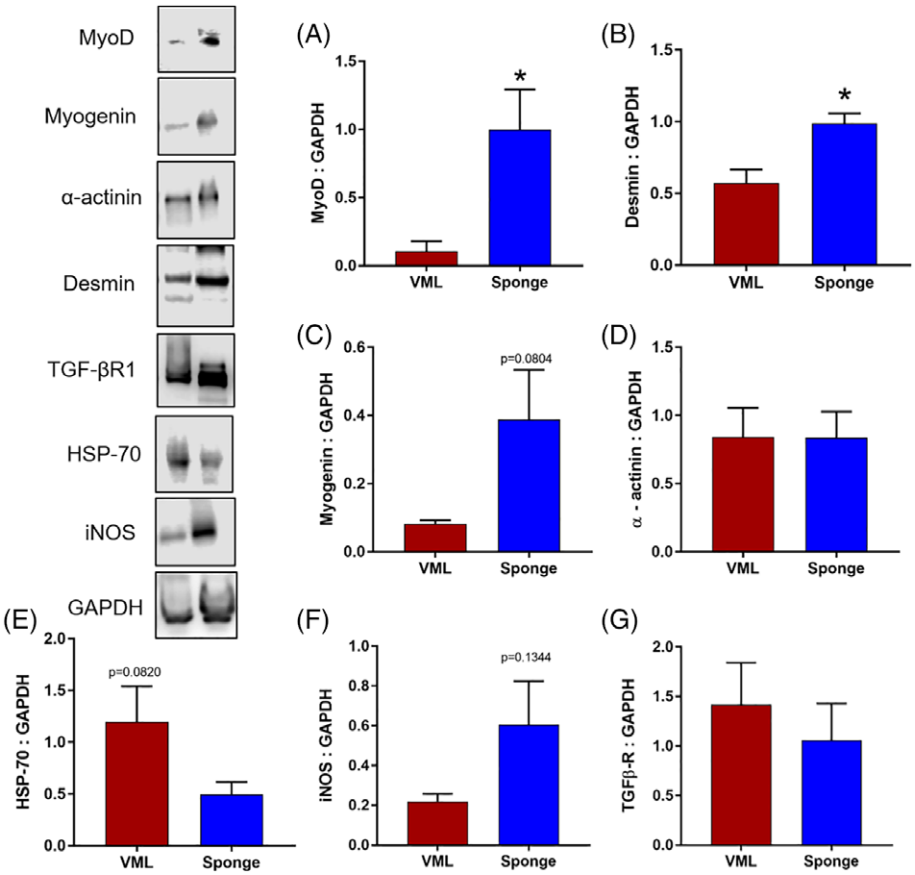

FIGURE 8. Quantitative analysis of biomimetic sponge mediated myogenesis in VML injured muscle was performed by western blotting analysis of (A) MyoD, (B) Desmin, (C) myogenin, (D) α-actinin, (E) HSP-70, (F) iNOS, and (G) TGF-β1R.

in the 70:30 biomimetic sponges may have also provided greater flexibility to the sponges, resulting in reduced compressive modulus [Fig. 3(C)]. Mechanical testing revealed that the stiffness of the hydrated scaffolds was orders of magnitude lower than the dry scaffolds, corroborating previous reports.[13] It has been suggested that in a hydrated state, scaffolds tend to buckle and bend at low stress, resulting in large deflections under small applied loads. Overall, these results suggest that the biomimetic sponges possess a large enough pore-size to allow cellular infiltration as well as adequate mechanical strength to serve a temporary scaffold at the site of injury *in vivo.* A homogenous spatial distribution of cells in the biomimetic sponges is expected to result in uniform ECM deposition, constructive remodeling, and *de novo* tissue formation upon implantation *in vivo.*

The myogenic potential of the biomimetic sponges was evaluated by quantifying the expression of myogenic proteins such as MyoD, myogenin, and α-actinin. On day 1 of culture, the expression of MyoD [Fig. 5(B)] trended higher while that of myogenin [Fig. 5(C)] was significantly higher on the 90:10 and 70:30 biomimetic sponges compared to the 100:0 gelatin sponges. The expression of α-actinin was significantly higher on the 90:10 sponge on day 1 compared to pure gelatin sponges. No significant differences were observed on day 5 between the sponges, indicating that the absence of collagen delayed myogenic activity in the 100:0 gelatin sponges. In support, previous studies have shown that pure gelatin scaffolds lack adequate bioactivity to influence fibroblast[28] and myogenic cell[50] infiltration.

To determine the effect of these sponges on myoblast activity, we quantified the cell-secreted factors. VEGF is a growth factor associated with myoblast proliferation and angiogenesis. VEGF receptors are upregulated in proliferating and differentiating satellite cells *in vitro.* VEGF also promotes myofiber growth and rescues myogenic cells from apoptosis.[52] Our results show that 70:30 biomimetic sponges produce the highest levels of VEGF on both days 1 and 5 of culture, suggesting that implantation of these sponges is likely to support angiogenesis and myogenic cell-proliferation in the injury region [Fig. 6(A)]. IGF-1 is a growth factor implicated in both proliferation and differentiation of myoblasts.[53] IGF-1 accumulates in regenerating muscle and is believed to coordinate the myogenic events at the injury site.[54,55] The levels of IGF-1 trended higher on the 70:30 biomimetic sponges compared to pure gelatin sponges on day 1 of culture, suggesting higher potential to influence myogenic activity. IL-6 is a pro-inflammatory cytokine that is highly expressed in actively contracting muscle fibers after increased workload.[56–59] An acute increase in pro-inflammatory factors such as IL-6 can serve as a chemoattractant for myoblasts and myeloid cells and support myoblast proliferation.[60] In addition, IL-6 deficiency is also known to cause blunted hypertrophic growth in

mice in response to mechanical overload.[58] Our results showed significantly higher production of IL-6 by myoblasts cultured on the 70:30 biomimetic sponges on both days 1 and 5, suggesting an increased capacity for cellular recruitment and myogenic cell proliferation. Taken together, these results show that biomimetic sponges are capable of promoting greater myogenic activity in C_2C_{12} myoblasts compared to pure gelatin sponges.

Based on the results of the *in vitro* studies, we selected the 70:30 biomimetic sponge for implantation in a mouse VML model.[38,39,61–64] It is known that muscle tissue retains the ability to regenerate after injury. However, this process is slow and often incomplete in traumatic injuries such as VML.[38,65] The early host response to implanted scaffolds typically determines successful tissue regeneration. At 2 weeks post-injury, the biomimetic sponge treated VML injured muscles showed constructive remodeling at the site of injury with the elevated presence of satellite ($Pax7^+$), endothelial ($CD31^+$) and inflammatory ($F4/80^+$) cells (Fig. 7). The ECM proteins in the biomimetic sponges may have potentially facilitated increased cellular recruitment, attachment, and proliferation. This result was encouraging since coordinated efforts by multiple cell populations are required for effective tissue repair and regeneration.[39,61] For instance, endothelial cells exert promitotic effect on myogenic progenitors and support the growth of satellite-cell derived myoblasts.[66] Macrophages are the key cellular players of the innate immune system that infiltrate the site of injury and scaffold implantation within 24–72 hours.[60] They secrete a wide variety of growth factors and cytokines that can influence myogenic events such as activation, proliferation, and fusion of myogenic precursors.[67]

The sponge treated VML injured muscles showed several small diameter $myosin^+$ myofibers in close proximity to the remaining muscle mass. In support, the protein expression of MyoD and desmin was significantly higher, while that of myogenin trended higher on the sponge treated injured muscles (Fig. 8). Taken together, these results suggest that compared to untreated muscles, the implantation of the biomimetic sponges results in greater myogenic activity in the VML injured muscles. As no statistical differences were noted in the quantitative analysis of collagen : myosin ratio as well as the number of myofibers with centrally located nuclei, we speculate that biomimetic sponge treated VML injured muscles are in the early stages of repair at the 2 week time-point and perhaps a longer duration of time would be required for significant myofiber regeneration throughout the defect region.

Muscle injury is often accompanied by an increase in HSP-70, which is released from cells following stress or injury and can activate the innate immune system.[44,45] However, this stress response peaks within the first 24 hours and is transient. The prolonged presence of HSPs may alter protein homeostasis and affect a variety of cellular functions.[68] The lower expression of HSP-70 in the biomimetic sponge treated muscles would suggest reduced cellular stress levels in the VML defect. The $F4/80^+$ macrophages infiltrating the VML defect are likely to be the primary population of cells expressing iNOS. Although iNOS is a marker for pro-inflammatory macrophages,[69] a previous study showed that that iNOS expression by infiltrating macrophages contributes to muscle regeneration and that myogenic precursor cells in the injured muscles of iNOS deficient mice failed to proliferate and differentiate.[46] The lack of arginase expression in both VML and biomimetic sponge treated muscles was surprising. It would suggest that the macrophages in the injured muscles have not progressed to an anti-inflammatory or pro-regenerative phenotype at the 2-week time-point. To further examine the effect on sponges on the host inflammatory response, we quantified the protein expression of TGF-β1 receptor. TGF-β1 is an anti-inflammatory factor that inhibits the function of both innate and adaptive immune cells by binding to TGF-β1 receptor on their cell surface.[70–73] The expression of TGF-βR1 was similar in both untreated and sponge treated VML muscles. Collectively, these data would suggest that the sponges are not causing any adverse inflammatory reaction or skewing the polarization of macrophages toward a distinct M1 or M2-like phenotype. However, a thorough analysis with a panel of several different pro-and anti-inflammatory markers is needed to further delineate the inflammatory response to the biomimetic sponges.

Although significant myofiber regeneration was not observed with biomimetic sponge treatment, we are encouraged by the fact that implantation of the biomimetic sponge recruited host cells into the defect region and increased myogenic activity in the VML injured muscles without causing any adverse inflammatory reactions or fibrotic capsule formation. It can be speculated that the biomimetic sponges possibly protected the remaining muscle mass from chronic injury, by providing both bioactivity and mechanical stability. The animal study was performed to characterize the *in vivo* response to biomimetic sponge implantation. A major limitation of the study is that the findings are preliminary as only one time-point was used for analysis. Future studies will determine the extent to which biomimetic sponge therapy can promote myofiber regeneration, innervation, and force production at 4 weeks post-injury. These studies will provide conclusive evidence regarding the success/failure of the biomimetic sponge therapy. As robust myofiber regeneration was not observed throughout the defect region, future studies may also consider loading biomimetic sponges with immunomodulatory molecules or pro-myogenic growth factors to accelerate myofiber regeneration. The development of an effective tissue engineering therapy for skeletal muscle may also benefit reconstructive surgery as well as congenital and degenerative muscle diseases.[12]

REFERENCES

1. Cross JD, Ficke JR, Hsu JR, Masini BD, Wenke JC. Battlefield orthopaedic injuries cause the majority of long-term disabilities. J Am Acad Orthop Surg 2011;19(Suppl 1):S1–S7.
2. Bowyer G. *Debridement of extremity war wounds*. J Am Acad Orthop Surg 2006;14(10):S52–S56.
3. Mannion SJ, Chaloner E. Principles of war surgery. BMJ 2005; 330(7506):1498–1500.
4. Sicari BM, Agrawal V, Siu BF, Medberry CJ, Dearth CL, Turner NJ, Badylak SF. A murine model of volumetric muscle loss and a

regenerative medicine approach for tissue replacement. Tissue Eng Part A 2012;18(19–20):1941–1948.
5. Corona BT, Rivera JC, Owens JG, Wenke JC, Rathbone CR. Volumetric muscle loss leads to permanent disability following extremity trauma. J Rehabil Res Dev 2015;52(7):785–792.
6. Grinsell D, Keating CP. Peripheral nerve reconstruction after injury: A review of clinical and experimental therapies. Biomed Res Int 2014;2014:698256.
7. Hirunsai M, Srikuea R, Yimlamai T. Heat stress promotes extracellular matrix remodelling via TGF-beta1 and MMP-2/TIMP-2 modulation in tenotomised soleus and plantaris muscles. Int J Hyperth 2015;31(4):336–348.
8. Smeele KM, Eerbeek O, Schaart G, Koeman A, Bezemer R, Nelson JK, Ince C, Nederlof R, Boek M, Laakso M, de Haan A, Drost MR, Hollmann MW, Zuurbier CJ. Reduced hexokinase II impairs muscle function 2 wk after ischemia-reperfusion through increased cell necrosis and fibrosis. J Appl Physiol 2012;113(4):608–618.
9. Roberts CS, Adams EL. The classification of open fractures: Are we there yet? Injury 2013;44(4):403–405.
10. Okano T, Matsuda T. Hybrid muscular tissues: Preparation of skeletal muscle cell-incorporated collagen gels. Cell Transplant 1997; 6(2):109–118.
11. Choi JS, Lee SJ, Christ GJ, Atala A, Yoo JJ. The influence of electrospun aligned poly(epsilon-caprolactone)/collagen nanofiber meshes on the formation of self-aligned skeletal muscle myotubes. Biomaterials 2008;29(19):2899–2906.
12. Beier JP, Klumpp D, Rudisile M, Dersch R, Wendorff JH, Bleiziffer O, Arkudas A, Polykandriotis E, Horch RE, Kneser U. Collagen matrices from sponge to nano: New perspectives for tissue engineering of skeletal muscle. BMC Biotechnol 2009;9:34.
13. Varley MC, Neelakantan S, Clyne TW, Dean J, Brooks RA, Markaki AE. Cell structure, stiffness and permeability of freeze-dried collagen scaffolds in dry and hydrated states. Acta Biomater 2016;33:166–175.
14. Le Grand F, Rudnicki MA. Skeletal muscle satellite cells and adult myogenesis. Curr Opin Cell Biol 2007;19(6):628–633.
15. Burkin DJ, Kim JE, Gu M, Kaufman SJ. Laminin and alpha7beta1 integrin regulate agrin-induced clustering of acetylcholine receptors. J Cell Sci 2000;113(Pt 16):2877–2886.
16. Wong TS, Booth FW. Skeletal muscle enlargement with weight-lifting exercise by rats. J Appl Physiol (1985) 1988;65(2):950–954.
17. Maffiuletti NA, Roig M, Karatzanos E, Nanas S. Neuromuscular electrical stimulation for preventing skeletal-muscle weakness and wasting in critically ill patients: A systematic review. BMC Med 2013;11:137.
18. Willand MP, Rosa E, Michalski B, Zhang JJ, Gordon T, Fahnestock M, Borschel GH. Electrical muscle stimulation elevates intramuscular BDNF and GDNF mRNA following peripheral nerve injury and repair in rats. Neuroscience 2016;334:93–104.
19. Hamrick MW. A role for myokines in muscle-bone interactions. Exerc Sport Sci Rev 2011;39(1):43–47.
20. Rooney JE, Gurpur PB, Burkin DJ. Laminin-111 protein therapy prevents muscle disease in the mdx mouse model for Duchenne muscular dystrophy. Proc Natl Acad Sci U S A 2009;106(19):7991–7996.
21. Van Ry PM, Minogue P, Hodges BL, Burkin DJ. Laminin-111 improves muscle repair in a mouse model of merosin-deficient congenital muscular dystrophy. Hum Mol Genet 2013;23(2):383–396.
22. Goudenege S, Lamarre Y, Dumont N, Rousseau J, Frenette J, Skuk D, Tremblay JP. Laminin-111: A potential therapeutic agent for Duchenne muscular dystrophy. Mol Ther 2010;18(12):2155–2163.
23. Zou K, de Lisio M, Huntsman HD, Pincu Y, Mahmassani Z, Miller M, Olatunbosun D, Jensen T, Boppart MD. Laminin-111 improves skeletal muscle stem cell quantity and function following eccentric exercise. Stem Cells Transl Med 2014;3(9):1013–1022.
24. Talovic M, Marcinczyk M, Ziemkiewicz N, Garg K. Laminin Enriched Scaffolds for Tissue Engineering Applications. Adv in Tissue Eng Regen Med 2017;2(3):00033.
25. Marcinczyk M, Elmashhady H, Talovic M, Dunn A, Bugis F, Garg K. Laminin-111 enriched fibrin hydrogels for skeletal muscle regeneration. Biomaterials 2017;141:233–242.
26. Rodriguez IA, Sell SA, McCool JM, Saxena G, Spence AJ, Bowlin GL. A preliminary evaluation of lyophilized gelatin sponges, enhanced with platelet-rich plasma, hydroxyapatite and chitin whiskers for bone regeneration. Cell 2013;2(2):244–265.
27. Hiwatashi N, Hirano S, Mizuta M, Tateya I, Kanemaru SI, Nakamura T, Ito J, Kawai K, Suzuki S. Biocompatibility and efficacy of collagen/gelatin sponge scaffold with sustained release of basic fibroblast growth factor on vocal fold fibroblasts in 3-dimensional culture. Ann Otol Rhinol Laryngol 2015;124(2):116–125.
28. Takemoto S, Morimoto N, Kimura Y, Taira T, Kitagawa T, Tomihata K, Tabata Y, Suzuki S. Preparation of collagen/gelatin sponge scaffold for sustained release of bFGF. Tissue Eng Part A 2008;14(10):1629–1638.
29. Ponticiello MS, Schinagl RM, Kadiyala S, Barry FP. Gelatin-based resorbable sponge as a carrier matrix for human mesenchymal stem cells in cartilage regeneration therapy. J Biomed Mater Res 2000;52(2):246–255.
30. Imani R, Rafienia M, Emami SH. Synthesis and characterization of glutaraldehyde-based crosslinked gelatin as a local hemostat sponge in surgery: An in vitro study. Biomed Mater Eng 2013;23(3): 211–224.
31. Choi YS, Hong SR, Lee YM, Song KW, Park MH, Nam YS. Study on gelatin-containing artificial skin: I. preparation and characteristics of novel gelatin-alginate sponge. Biomaterials 1999;20(5):409–417.
32. Barnes CP, Pemble CW IV, Brand DD, Simpson DG, Bowlin GL. Cross-linking electrospun type II collagen tissue engineering scaffolds with carbodiimide in ethanol. Tissue Eng 2007;13(7): 1593–1605.
33. Schoof H, Apel J, Heschel I, Rau G. Control of pore structure and size in freeze-dried collagen sponges. J Biomed Mater Res 2001; 58(4):352–357.
34. Lu H, Ko YG, Kawazoe N, Chen G. Cartilage tissue engineering using funnel-like collagen sponges prepared with embossing ice particulate templates. Biomaterials 2010;31(22):5825–5835.
35. Hixon KR, Lu T, McBride-Gagyi SH, Janowiak BE, Sell SA. A comparison of tissue engineering scaffolds incorporated with Manuka honey of varying UMF. Biomed Res Int 2017;2017:4843065.
36. Hixon KR, Eberlin CT, Kadakia PU, McBride-Gagyi SH, Jain E, Sell SA. A comparison of cryogel scaffolds to identify an appropriate structure for promoting bone regeneration. Biomed Phy Engine Exp 2016;2(3):035014.
37. Kuo ZK, Lai PL, Toh EKW, Weng CH, Tseng HW, Chang PZ, Chen CC, Cheng CM. Osteogenic differentiation of preosteoblasts on a hemostatic gelatin sponge. Sci Rep 2016;6:32884.
38. Garg K, Corona BT, Walters TJ. Losartan administration reduces fibrosis but hinders functional recovery after volumetric muscle loss injury. J Appl Physiol (1985) 2014;117(10):1120–1131.
39. Garg K, Ward CL, Rathbone CR, Corona BT. Transplantation of devitalized muscle scaffolds is insufficient for appreciable de novo muscle fiber regeneration after volumetric muscle loss injury. Cell Tissue Res 2014;358(3):857–873.
40. Pejnovic NN, Pantic JM, Jovanovic IP, Radosavljevic GD, Milovanovic MZ, Nikolic IG, Zdravkovic NS, Djukic AL, Arsenijevic NN, Lukic ML. Galectin-3 deficiency accelerates high-fat diet-induced obesity and amplifies inflammation in adipose tissue and pancreatic islets. Diabetes 2013;62(6):1932–1944.
41. Nguyen-Thanh T, Kim D, Lee S, Kim W, Park SK, Kang KP. Inhibition of histone deacetylase 1 ameliorates renal tubulointerstitial fibrosis via modulation of inflammation and extracellular matrix gene transcription in mice. Int J Mol Med 2018;41(1): 95–106.
42. Fuoco C, Sangalli E, Vono R, Testa S, Sacchetti B, Latronico MV, Bernardini S, Madeddu P, Cesareni G, Seliktar D, Rizzi R, Bearzi C, Cannata SM, Spinett G, Gargioli C. 3D hydrogel environment rejuvenates aged pericytes for skeletal muscle tissue engineering. Front Physiol 2014;5:203.
43. Sacco A, Doyonnas R, Kraft P, Vitorovic S, Blau HM. Self-renewal and expansion of single transplanted muscle stem cells. Nature 2008;456(7221):502–506.
44. Liu Y, Gampert L, Nething K, Steinacker JM. Response and function of skeletal muscle heat shock protein 70. Front Biosci 2006;11: 2802–2827.
45. Senf SM. Skeletal muscle heat shock protein 70: Diverse functions and therapeutic potential for wasting disorders. Front Physiol 2013; 4:330.
46. Rigamonti E, Touvier T, Clementi E, Manfredi AA, Brunelli S, Rovere-Querini P. Requirement of inducible nitric oxide synthase

for skeletal muscle regeneration after acute damage. J Immunol 2013;190(4):1767–1777.
47. Aurora A, Corona BT, Walters TJ. A porcine urinary bladder matrix does not recapitulate the spatiotemporal macrophage response of muscle regeneration after volumetric muscle loss injury. Cells Tissues Organs 2016;202(3–4):189–201.
48. Aurora A, Roe JL, Corona BT, Walters TJ. An acellular biologic scaffold does not regenerate appreciable de novo muscle tissue in rat models of volumetric muscle loss injury. Biomaterials 2015;67: 393–407.
49. Goldman SM, Henderson BEP, Walters TJ, Corona BT. Co-delivery of a laminin-111 supplemented hyaluronic acid based hydrogel with minced muscle graft in the treatment of volumetric muscle loss injury. PLoS One 2018;13(1):e0191245.
50. Ju YM, Atala A, Yoo JJ, Lee SJ. In situ regeneration of skeletal muscle tissue through host cell recruitment. Acta Biomater 2014; 10(10):4332–4339.
51. Park H, Guo X, Temenoff JS, Tabata Y, Caplan AI, Kasper FK, Mikos AG. Effect of swelling ratio of injectable hydrogel composites on chondrogenic differentiation of encapsulated rabbit marrow mesenchymal stem cells in vitro. Biomacromolecules 2009;10(3):541–546.
52. Arsic N, Zacchigna S, Zentilin L, Ramirez-Correa G, Pattarini L, Salvi A, Sinagra G, Giacca M. Vascular endothelial growth factor stimulates skeletal muscle regeneration in vivo. Mol Ther 2004; 10(5):844–854.
53. Engert JC, Berglund EB, Rosenthal N. Proliferation precedes differentiation in IGF-I-stimulated myogenesis. J Cell Biol 1996;135(2): 431–440.
54. Edwall D, Schalling M, Jennische E, Norstedt G. Induction of insulin-like growth factor I messenger ribonucleic acid during regeneration of rat skeletal muscle. Endocrinology 1989;124(2): 820–825.
55. Jennische E, Hansson HA. Regenerating skeletal muscle cells express insulin-like growth factor I. Acta Physiol Scand 1987;130(2): 327–332.
56. Carson JA, Baltgalvis KA. Interleukin 6 as a key regulator of muscle mass during cachexia. Exerc Sport Sci Rev 2010;38(4):168–176.
57. Kami K, Morikawa Y, Sekimoto M, Senba E. Gene expression of receptors for IL-6, LIF, and CNTF in regenerating skeletal muscles. J Histochem Cytochem 2000;48(9):1203–1213.
58. Serrano AL, Baeza-Raja B, Perdiguero E, Jardí M, Muñoz-Cánoves P. Interleukin-6 is an essential regulator of satellite cell-mediated skeletal muscle hypertrophy. Cell Metab 2008;7(1):33–44.
59. White JP, Reecy JM, Washington TA, Sato S, le ME, Davis JM, Wilson LB, Carson JA. Overload-induced skeletal muscle extracellular matrix remodelling and myofibre growth in mice lacking IL-6. Acta Physiol (Oxf) 2009;197(4):321–332.
60. Tidball JG, Villalta SA. Regulatory interactions between muscle and the immune system during muscle regeneration. Am J Physiol Regul Integr Comp Physiol 2010;298(5):R1173–R1187.
61. Corona BT, Garg K, Ward CL, McDaniel JS, Walters TJ, Rathbone CR. Autologous minced muscle grafts: A tissue engineering therapy for the volumetric loss of skeletal muscle. Am J Physiol Cell Physiol 2013;305(7):C761–C775.
62. Garg K, Ward CL, Hurtgen BJ, Wilken JM, Stinner DJ, Wenke JC, Owens JG, Corona BT. Volumetric muscle loss: Persistent functional deficits beyond frank loss of tissue. J Orthop Res 2015;33(1): 40–46.
63. Hurtgen BJ, Pollot BE, Ward CL, Goldman SM, Garg K, McKinley TO, Greising SM, Wenke JC, Corona BT. FK506 restores fracture healing that is impaired by concomitant skeletal muscle trauma. BMC Musculoskelet Disord 2017;18:253. Accepted for publication.
64. Hurtgen BJ, Ward CL, Garg K, Pollot BE, Goldman SM, McKinley T, Wenke JC, Corona BT. Severe muscle trauma triggers heightened and prolonged local musculoskeletal inflammation and impairs adjacent tibia fracture healing. J Musculoskelet Neuronal Interact 2016;16(2):122–134.
65. Lieber RL, Ward SR. Cellular mechanisms of tissue fibrosis. 4. Structural and functional consequences of skeletal muscle fibrosis. Am J Physiol Cell Physiol 2013;305(3):C241–C252.
66. Bentzinger CF, Wang YX, Dumont NA, Rudnicki MA. Cellular dynamics in the muscle satellite cell niche. EMBO Rep 2013;14(12): 1062–1072.
67. Saclier M, Yacoub-Youssef H, Mackey AL, Arnold L, Ardjoune H, Magnan M, Sailhan F, Chelly J, Pavlath GK, Mounier R, Kjaer M, Chazaud B. Differentially activated macrophages orchestrate myogenic precursor cell fate during human skeletal muscle regeneration. Stem Cells 2013;31(2):384–396.
68. Pockley AG. Heat shock proteins, inflammation, and cardiovascular disease. Circulation 2002;105(8):1012–1017.
69. Garg K, Pullen NA, Oskeritzian CA, Ryan JJ, Bowlin GL. Macrophage functional polarization (M1/M2) in response to varying fiber and pore dimensions of electrospun scaffolds. Biomaterials 2013; 34(18):4439–4451.
70. Chen Y, Kam CSK, Liu FQ, Liu Y, Lui VCH, Lamb JR, Tam PKH. LPS-induced up-regulation of TGF-beta receptor 1 is associated with TNF-alpha expression in human monocyte-derived macrophages. J Leukoc Biol 2008;83(5):1165–1173.
71. de Boer WI et al. Transforming growth factor beta1 and recruitment of macrophages and mast cells in airways in chronic obstructive pulmonary disease. Am J Respir Crit Care Med 1998;158(6):1951–1957.
72. Ellingsworth L, Nakayama D, Dasch J, Segarini P, Carrillo P, Waegell W. Transforming growth factor beta 1 (TGF-beta 1) receptor expression on resting and mitogen-activated T cells. J Cell Biochem 1989;39(4):489–500.
73. Schmidt-Weber CB, Letarte M, Kunzmann S, Rückert B, Bernabéu C, Blaser K. TGF-{beta} signaling of human T cells is modulated by the ancillary TGF-{beta} receptor endoglin. Int Immunol 2005;17(7):921–930.